Fungal Genetics and Biology 60 (2013) 87–100

Contents lists available at ScienceDirect

Fungal Genetics and Biology

journal homepage: www.elsevier.com/locate/yfgbi

Comparative proteomics in the genus *Paracoccidioides*

Laurine Lacerda Pigosso [a], Ana Flávia Alves Parente [a], Alexandre Siqueira Guedes Coelho [b], Luciano Paulino Silva [c], Clayton Luiz Borges [a], Alexandre Melo Bailão [a], Célia Maria de Almeida Soares [a,*]

[a] Laboratório de Biologia Molecular, Instituto de Ciências Biológicas, Universidade Federal de Goiás, Goiânia, GO, Brazil
[b] Laboratório de Genética e Genômica de Plantas, Escola de Agronomia, Universidade Federal de Goiás, Goiânia, GO, Brazil
[c] Laboratório de Espectrometria Massas, Centro Nacional de Pesquisa de Recursos Genéticos e Biotecnologia, Empresa Brasileira de Pesquisa Agropecuária, Brasília, DF, Brazil

ARTICLE INFO

Article history:
Available online 31 July 2013

Keywords:
Paracoccidioides
Phylogenetic species
Comparative proteomic profiles

ABSTRACT

The genus *Paracoccidioides* comprises a complex of phylogenetic species of dimorphic pathogenic fungi, the etiologic agents of paracoccidioidomycosis (PCM), a disease confined to Latin America and of marked relevance in its endemic areas due to its high frequency and severity. The members of the *Paracoccidioides* genus are distributed in distinct phylogenetic species (*S1, PS2, PS3* and *01-like*) that potentially differ in their biochemical and molecular characteristics. In this work, we performed the proteomic characterization of different members of the genus *Paracoccidioides.* We compared the proteomic profiles of *Pb*01 (*01-like*), *Pb*2 (*PS2*), *Pb*339 (*S1*) and *Pb*EPM83 (*PS3*) using 2D electrophoresis and mass spectrometry. The proteins/isoforms were selected based on the staining intensity of the spots as determined by image analysis. The proteins/isoforms were in-gel digested and identified by peptide mass fingerprinting and ion fragmentation. A total of 714 spots were detected, of which 343 were analyzed. From these spots, 301 represented differentially expressed proteins/isoforms among the four analyzed isolates, as determined by ANOVA. After applying the FDR correction, a total of 267 spots were determined to be differentially expressed. From the total, 193 proteins/isoforms were identified by PMF and confirmed by ion fragmentation. Comparing the expression profiles of the isolates, the proteins/isoforms that were related to glycolysis/gluconeogenesis and to alcohol fermentation were more abundant in *Pb*01 than in other representatives of the genus *Paracoccidioides,* indicating ahigher use of anaerobic pathways for energy production. Those enzymes related to the oxidative stress response were more abundant in *Pb*01, *Pb*2 and *Pb*339, indicating a better response to ROS in these members of the *Paracoccidioides* complex. The enzymes of the pentose phosphate pathway were abundant in *Pb*2. Antigenic proteins, such as GP43 and a 27-kDa antigenic protein, were less abundant in *Pb*01 and *Pb*2. The proteomic profile indicates metabolic differences among the analyzed members of the *Paracoccidioides* genus.

1. Introduction

The genus *Paracoccidioides* comprises thermally dimorphic pathogens from the family Ajellomycetaceae, order *Onygenales* (Untereiner et al., 2004). Those human pathogens are the etiological agents of paracoccidioidomycosis (PCM), one of the most frequent systemic mycoses that affect rural populations in Latin America (Restrepo and Tobon, 2005). The fungus is found in nature as mycelium and in the human host in the form of yeast. The mycelia-to-yeast morphological transition is triggered by temperature, and this event is essential to the establishment of the infection (San-Blas et al., 2002). The infection begins with the inhalation of fungal propagules, which reach the epithelium of the alveoli, where they differentiate into the pathogenic yeastform. Although most clinical forms of the disease are asymptomatic, severe and progressive infections occur, involving pulmonary and extrapulmonary tissues, such as the skin, lymph nodes, oropharyngeal mucosa, adrenal gland and central nervous system (Brummer et al., 1993; Franco, 1987; Restrepo et al., 2001). A Multi-Locus Sequencing Typing (MLST) analysis revealed the existence of four cryptic species in the *Paracoccidioides* genus: *S1, PS2* and *PS3* from the *Paracoccidioides. brasiliensis* complex and *P. lutzii* harboring *Pb01-like* isolates (Teixeira et al., 2009; Matute et al., 2006).

The availability of sequenced and annotated genomes of members of the *Paracoccidioides* genus (isolates *Pb*01, *Pb*18 and *Pb*3) in the Dimorphic Fungal Database of the Broad Institute site (http://www.broadinstitute.org/annotation/genome/dimoph_collab/MultiHome.html) provided a good start to compare the members of this genus and to better understand the biology of these medically significant fungi. Due to subtle or inexistent morphological differences among cryptic species, molecular techniques have

* Corresponding author. Address: Laboratório de Biologia Molecular, Instituto de Ciências Biológicas, ICBII, Campus II, Universidade Federal de Goiás, 74001-970, Goiânia, Goiás, Brazil. Fax: +55 62 35211110.
E-mail address: cmasoares@gmail.com (C.M.A. Soares).

1087-1845/$ - see front matter © 2013 Elsevier Inc. All rights reserved.
http://dx.doi.org/10.1016/j.fgb.2013.07.008

become the tools of choice in distinguishing between such members (Teixeira et al., 2009; Theodoro et al., 2008). Although no differences in disease manifestation have been described, the phylogenetic species differ in genome size (29.1–32.9 Mb) and in the number of genes (7610–8130) (Desjardins et al., 2011).

With plenty of genomic information for *Paracoccidioides*, further functional research can provide more information at protein level. So far, few studies have been published regarding the proteomics of *Paracoccidioides*. Attempts have been made by our group in characterizing the proteome of *Paracoccidioides* (*Pb*01) which have helped in elucidating the proteins that are associated with the fungus phase transition (Rezende et al., 2011), the fungal response to iron and zinc starvation (Parente et al., 2011, 2013) and the secretomes of yeast and mycelia (Weber et al., 2012), as well as the fungal response to oxidative stress (Grossklaus et al., 2013). Those studies revealed the numerous and complex composition of proteins and identified molecules that are potentially relevant to the transition of the fungus to the yeast pathogenic phase and to the fungus adaptation to the host milieu, as well as to the *Paracoccidioides* interaction with the host. Proteomic studies have also focused on the proteomic composition of extracellular vesicles and the exoproteome of *Pb*18; these studies provided an overall view of the extracellular vesicle protein of this fungus (Vallejo et al., 2011).

There is still a lack of quantitative comparisons between the proteome maps of members of the *Paracoccidioides* complex. In this work, we used two-dimensional protein fractionation coupled with mass spectrometry to visualize the potential biological differences among members of the *Paracoccidioides* complex. Proteomic profiles were obtained for members of the following phylogenetic species: *P. lutzii* (*Pb*01) and *P. brasiliensis*: *Pb*2 (PS2), *Pb*339 (S1) and *Pb*Epm83 (PS3). A total of 714 protein spots were detected and 343 were analyzed. From these spots, 267 proteins/isoforms were differentially expressed greater than 1.5-fold. From the differentially expressed proteins spots, 193 were identified. A comparative analysis of the proteome revealed potential differential metabolic aspects among the members of the four phylogenetic lineages in the genus *Paracoccidioides*. To our knowledge, this is the first study using proteomics to investigate the potential biochemical differences among members of the *Paracoccidioides* genus.

2. Materials and methods

2.1. Strains and culture conditions

*Paracoccidioides Pb*01 (ATCC-MYA-826) (Parente et al., 2011; Weber et al., 2012), *Pb*2 (Matute et al., 2006), *Pb*339 (Matute et al., 2006) and *Pb*Epm83 (Theodoro et al., 2008) were used in this study. The yeast phase was maintained *in vitro* by subculturing at 36 °C in Fava Netto's semisolid medium [1% (w/v) peptone, 0.5% (w/v) yeast extract, 0.3% (w/v) proteose peptone, 0.5% (w/v) beef extract, 0.5% (w/v) NaCl, 4% (w/v) glucose, 1.2% (w/v) agar, pH 7.2] every 7 days.

2.2. Preparation of protein extracts

To obtain protein extracts, yeast cultures were prepared by inoculating 250 mL Fava Netto's liquid medium with 10^6 cells/mL incubated under agitation at 36 °C for 72 h. The cells were collected by centrifugation at 10,000*g* for 5 min, followed by the addition of extraction buffer (20 mM Tris–HCl pH 8.8; 2 mM $CaCl_2$) containing a mixture of nuclease and protease inhibitors (serine, cysteine and calpain) (GE Healthcare, Uppsala, Sweden). This suspension was distributed in tubes, glass beads were added, and the suspension was processed on ice in the bead beater (BioSpec, Oklahoma, USA) apparatus for 5 cycles of 30 s, followed by centrifugation at 10,000*g* for 15 min at the same temperature. The supernatant was collected, the protein concentrations were determined using the Bradford reagent (Sigma Aldrich, Co., St. Louis, MO), and bovine serum albumin (BSA) was used as a standard.

2.3. Two-dimensional gel electrophoresis

Equal amounts of proteins (300 μg of protein extract *per* gel) were loaded. The interfering molecules were removed by cleaning with the 2-D Clean-up Kit (GE Healthcare, Uppsala, Sweden) according to the manufacturer's instructions. The proteins were solubilized in 250 μL of buffer containing 7 M urea, 2 M thiourea, 130 mM 3-[(3-Cholamidopropyl)dimethylammonio]-1-propanesulfonate (CHAPS), 0.002% (w/v) dithiothreitol (DTT), ampholyte-containing buffer (IPG buffer, GE Healthcare) and traces of bromophenol blue (Shaw and Riederer, 2003). The samples were applied to 13-cm Immobiline™ DryStrip Gels (GE Healthcare) with a linear separation range of pH 3-11. Isoelectric focusing was successively conducted in a Ettan IPGphor 3 Electrophoresis system (GE Healthcare) at 30 V for 14 h, 500 V for 500 Vh (step), 1 kV for 800 Vh (gradient), 8 kV for 11.3 kVh (gradient) and 8 kV for 2.9 kVh (step) at a maximum setting of 50 μA per strip. As previously described (Herbert et al., 2001), after isoelectric focusing, the strips were kept in equilibration buffer [50 mM Tris–HCl pH 8.8, 6 M urea, 30% (v/v) glycerol, 2% (w/v) sodium dodecyl sulfate (SDS), and 0.002% (w/v) bromophenol blue] containing 18 mM DTT for 40 min. This step was followed by the incubation in equilibration buffer with 135 mM iodoacetamide for 40 min prior to polyacrylamide gel electrophoresis under denaturing conditions (SDS–PAGE) (Laemmli, 1970). The IPG strips were placed over the polyacrylamide gels and covered with agarose [0.5% (w/v) in running buffer containing 25 mM Tris–HCl, 192 mM glycine, 0.1% (w/v) SDS]. The SDS–PAGE of each experimental biological triplicate was simultaneously performed at 10 °C for 1 h at 150 V and 250 V until the front reached the gel end. The proteins were visualized by Coomassie brilliant blue staining (PlusOne Coomassie Tablets PhastGel Blue R-350, GE Healthcare) according to manufacturer's instructions.

2.4. Image analyses

The images of the Coomassie blue 2-D gels were scanned using Image Scanner III (GE Healthcare) using LabScan software (GE Healthcare) in transparent mode. The image analysis was performed with Image Master 2D Platinum v 6.0 (GE Healthcare). The gels were aligned, and the intensity of the spots was normalized and matched between different gels, procedures that were performed automatically using the Image Master software. The automated matching of the gels was checked manually and corrected if necessary. The spots were quantified and normalized using the volume criterion. For each spot, the volume percentage was calculated. The intensities of the Coomassie staining were normalized considering the standardized relative intensity volume of spots; this value is the volume of each spot divided by the total volume of all of the spots. The volume ratio values of the matched spots were used for statistical analyses.

2.5. Statistical analyses

The differences in protein expression levels among members of the phylogenetic groups were tested using the two-way ANOVA test. The FDR (False Discovery Rate) criterion was used for multiple comparisons for the correction of type I errors (less than 0.05). When declared statistically significant by ANOVA, the differences among the means were evaluated using Tukey's test. The statistical

analyses were performed using R software (http://www.r-project.org/). A *p*-value equal to or less than 0.05 was considered statistically significant.

The MultiExperiment Viewer software V.4.8 (www.tm4.org/mev/) was used to group the comparative proteomic data. To analyze the isolates, the up- and down-regulated proteins were combined and the expression levels that were estimated for each protein were used to build a heat map. In this way, the differences in the proteomic profiles were examined by hierarchical clustering using the Pearson correlation as a measure of similarity.

To analyze the data from enzymatic activities, statistical comparisons were performed using a two-way ANOVA, and, when declared statistically significant, the differences among the means were evaluated using Tukey's test.

To analyze the data regarding the oxidative stress and heat shock response, statistical comparisons were performed using Student's *t*-test. Samples with *p*-values <0.05 were considered statistically significant.

2.6. In-gel enzymatic digestion

The Coomassie blue-stained spots were manually excised from the gels and diced into small pieces. The gel pieces were washed twice with MilliQ H_2O and then dehydrated in 100 μL acetonitrile (ACN) and dried in a speed vacuum. The gel pieces were then reduced with 10 mM DTT and alkylated with 55 mM iodoacetamide. The supernatant was removed, and the gels were washed with 100 μL ammonium bicarbonate by vortexing for 10 min. The supernatant was removed, and the gel pieces were dehydrated in 100 μL of a solution containing 25 mM ammonium bicarbonate/50% ACN (v/v), vortexed for 5 min, and centrifuged. This step was repeated. The gel pieces were dried and a 12.5-ng/mL trypsin solution was added (Sequencing Grade Modified Trypsin Promega, Madison, WI, USA), followed by rehydration on ice at 4 °C for 10 min. The supernatant was removed, and to the gel pieces, 25 μL of a 25-mM solution of ammonium bicarbonate was added. This step was followed by incubation at 37 °C for 16 h. Following digestion, the supernatant was placed into a clean tube. To the gel pieces, 50 μL of a solution containing 50% (v/v) ACN, 5% (v/v) trifluoroacetic acid (TFA) were added. The samples were mixed for 10 min and sonicated for three cycles of 3 min, and the solution was then combined with the above aqueous extraction. The samples were dried in a speed vacuum, and the peptides were solubilized in water. Two microliters of each sample were delivered to a target plate and dried at room temperature. Next, the peptide mixtures were covered with 2 μL of 10 mg/mL alpha cyano-4-hydroxycinammic acid in 50% (v/v) ACN, 5% (v/v) TFA. A concentration and a purification step using a pipette tip with a bed of chromatographic media (ZipTips® C18 Pipette Tips, Millipore, Bedford, MA, USA) was used to favor the identification of less abundant proteins.

2.7. Mass spectrometry analysis

The peptides that were obtained by the in-gel digestion were analyzed by PMF and MS/MS in a matrix-assisted laser desorption/ionization (MALDI) quadrupole, time-of-flight (Q-TOF) mass spectrometer (MS) (Synapt, Waters, Manchester, UK). The mass spectra were performed using the Mass Lynx (Waters) software. The raw data were processed using the Protein Lynx Global Server software (version 2.1, Micromass/Waters). Both the resulting peptide mass and the associated fragmentation spectra were submitted to MASCOT software (www.matrixscience.com). The searches were performed against an NCBI non-redundant database with a 100-ppm mass tolerance. The searches were performed without a constraining protein molecular weight or isoelectric point, with variable carbamidomethylation of cysteine and oxidation of methionine residues. The search parameters were restricted to fungi and allowed for one missed cleavage. The proteins were identified by comparing the collected data with the NCBI databank (http://www.ncbi.nlm.nih.gov/).

2.8. Formamidase activity assay

The formamidase activity was measured by monitoring ammonia formation, as previously described (Borges et al., 2010). One microgram of the total protein extract was added to 200 μL of the formamide substrate solution at a 100-mM final concentration in 100 mM phosphate buffer, pH 7.4, and 10 mM EDTA. The reaction mixture was incubated at 37 °C for 30 min, followed by the addition of 400 μL phenol-nitroprusside and 400 μL alkaline hypochlorite (Sigma Aldrich, Co.). The samples were incubated for 6 min at 50 °C, and the absorbance was read at 625 nm. The amount of released ammonia was determined from a standard curve. One unit (U) of formamidase-specific activity was defined as the amount of enzyme required to hydrolyze 1 μmol of formamide (corresponding to the formation of 1 μmol of ammonia) per min per mg of total protein.

2.9. Measurement of the intracellular NADPH /$NADP^+$

The intracellular $NADP^+$ and NADPH concentrations were measured using the NADP/NADPH Assay Kit (Abcam, Cambridge, UK) according to the manufacturer's instructions. Briefly, the *Paracoccidioides* yeast cells were collected and washed with PBS. After centrifugation, the cells (10^8) were resuspended in 400 μL NADP/NADPH extraction buffer. Glass beads were added, and the suspension was processed on ice in the bead beater (BioSpec, Oklahoma, USA) for 3 cycles of 30 s. After centrifugation, the supernatants were diluted 5× and used to perform the NADP + and NADPH quantifications. The quantifications were performed in a 96-well microplate reader at 450 nm. The experiment was performed in three independents replicates.

2.10. Ethanol measurement

The concentrations of ethanol in the cultures were quantified using the enzymatic detection kit, a UV-test for ethanol, (R-Biopharm, Darmstadt, Germany), according to the manufacturer's instructions. Ethanol is oxidized to acetaldehyde by the enzyme alcohol dehydrogenase in the presence of nicotinamide adenine dinucleotide (NAD). Acetaldehyde is quantitatively oxidized to acetic acid in the presence of aldehyde dehydrogenase, releasing NADH, the amount of which is determined by means of its absorbance at 340 nm. The yeast cells of the members of the *Paracoccidioides* complex (10^8 cells) were used in this assay. The cell suspension was distributed in tubes; glass beads were added, and the suspension was processed on ice in the bead beater (BioSpec, Oklahoma, USA) for 5 cycles of 30 s. The cell lysate was centrifuged at 10,000*g* for 15 min at 4 °C, and the supernatant was used for the enzymatic assay according to the manufacturer's instructions. The concentrations of ethanol were obtained in triplicate.

2.11. Response of Paracoccidioides to oxidative stress

The response to oxidative stress was investigated in yeast cells of *Paracoccidioides*. A total of 10^7 yeast cells/mL were exposed to 1 mM menadione (Sigma Aldrich, Co.) at 36 °C for 2, 4 and 6 h with agitation at 150 rpm as previously described (Grossklaus et al., 2013). The controls were obtained, and all of the experiments were performed in triplicate. The viability was determined by a membrane integrity analysis using propidium iodide as a marker for

dead cells. The cell suspension (10^6 yeast cells/mL) was centrifuged, and the supernatant was discarded. The cells were stained with the propidium iodide solution (1 mg/mL) for 20 min in the dark at room temperature. After dye incubation, the stained cell suspension was immediately analyzed in a C6 Accuri flow cytometer (Accuri Cytometers, Ann Arbor, MI, USA). A minimum of 5000 cells per sample was acquired with the FL3-H channel. The data were collected and analyzed using the FCS Express 4 Plus Research Edition software (De Novo Software, Los Angeles, CA, USA).

2.12. Response of Paracoccidioides to heat shock

A total of 10^6 yeast cells/mL of the *Paracoccidioides* isolates were subjected to different heat stress conditions (42 °C/1 h and 42 °C/2 h). The equivalent of 10^2 viable cells/mL was plated on BHI semisolid medium. The plates were incubated at 37 °C, and the number of colony forming units (CFUs) was determined after 7 days. The assay was performed in three independents replicates.

2.13. Growth of Paracoccidioides in different carbon sources

The isolates that were used in this study were grown at 36 °C in Fava Netto's liquid medium under gentle shaking for 72 h. The exponentially growing cultures of *Paracoccidioides* isolates were washed with sterile 0.9% (w/v) NaCl and resuspended in the same solution, and the number of cells was adjusted to 10^6/mL. Different volumes were spotted onto McVeigh/Morton medium (Restrepo and Jiménez, 1980) containing the carbon sources glucose or oleic acid, both at 20 mM. The plates were incubated for 7 to 15 days at 37 °C and photographed.

3. Results

3.1. Proteomic profiles of members of the Paracoccidioides complex

In this study, we applied a proteomic strategy to identify proteins that were preferentially expressed by the yeast phase in the following members of the *Paracoccidioides* complex: *Pb*01 (01-like), *Pb*339 (S1), *Pb*2 (PS2), and *Pb*EPM83 (PS3). The protein expression profiles of *Paracoccidioides* were obtained using 2D electrophoresis. Fig. 1 depicts the representative two-dimensional gel of the analyzed isolates that were performed in biological triplicates. The proteins spots with molecular weights ranging from 11.0 to 84 kDa and *p*I values between 3 and 11 were detected, as depicted. Nonetheless, these four selected species are a representative sample of the *Paracoccidioides* proteomic diversity. The qualitative and quantitative differences in the spots can be visualized, as depicted in Fig. 1.

A total of 714 spots were detected, and from those, 343 were analyzed, considering the four proteomes that were included for statistical analysis, as depicted in Fig. S1. A total of 343 spots were matched and assessed for statistical significance using an ANOVA

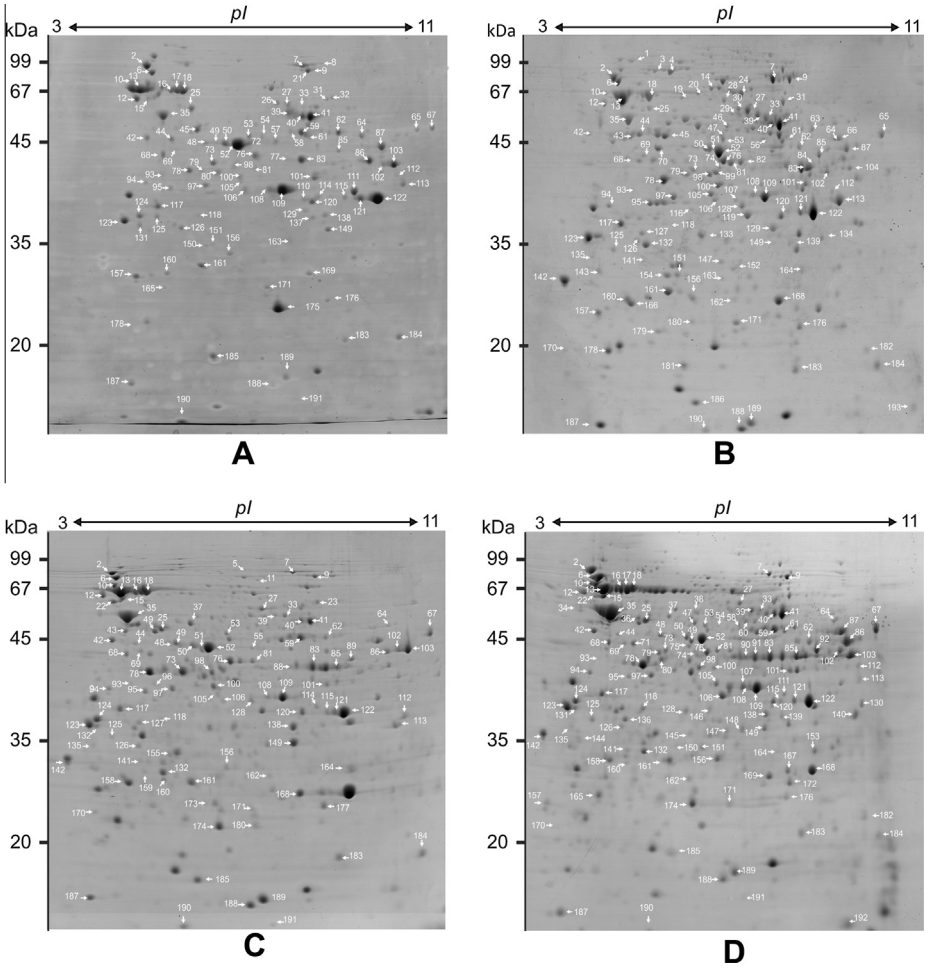

Fig. 1. Analysis of proteins from *Paracoccidioides* phylogenetic groups by two-dimensional gel electrophoresis: (A) *Pb*01; (B) *Pb*2; (C) *Pb*339; and (D) *Pb*EPM83. The proteins were extracted by mechanical cell rupture. Equal amounts of proteins were submitted to two-dimensional electrophoresis using ImmobilineZ DryStrip Gels for isoelectric focusing, followed by SDS–PAGE. The proteins were visualized by using Coomassie brilliant blue staining.

Table 1
Proteins/isoforms with increased abundance in *Pb*01.

Spot number[a]	Accession number[b]	Protein description	MW (kDa) Theo/Exp[c]	*p*I Theo/Exp[d]	*p*-value[e]
Energy					
Glycolysis and gluconeogenesis					
108	gi|29826036	Fructose 1,6-biphosphate aldolase 1	39.76/36.00	6.1/7.1	9.13E−03
109	gi|29826036	Fructose 1,6-biphosphate aldolase 1	39.76/36.10	6.1/7.3	7.96E−07
52	gi|146762537	Enolase	47.41/44.50	5.6/6.5	3.78E−06
50	gi|146762537	Enolase	47.41/45.90	5.6/6.2	8.51E−03
48	gi|146762537	Enolase	47.41/45.50	5.6/5.8	8.54E−06
122	gi|295658119	Glyceraldehyde-3-phosphate dehydrogenase	36.62/34.10	8.2/9.1	2.89E−03
115	gi|295658119	Glyceraldehyde-3-phosphate dehydrogenase	36.62/34.00	8.2/8.6	3.10E−04
121	gi|295658119	Glyceraldehyde-3-phosphate dehydrogenase	36.62/34.20	8.2/8.9	1.25E−02
161	gi|295670663	Triosephosphate isomerase	27.15/23.00	5.3/5.7	1.16E−02
83	gi|295669690	Phosphoglycerate kinase	45.31/42.00	6.4/7.7	5.10E−04
25	gi|295659988	2,3-bisphosphoglycerate-independent phosphoglycerate mutase	57.30/57.00	5.3/5.6	1.06E−04
26	gi|295662174	Pyruvate kinase	59.50/58.60	6.3/7.5	*
Tricarboxylic-acid pathway					
21	gi|225684009	Aconitase	85.06/78.60	7.2/7.9	*
Pentose-phosphate pathway					
110	gi|295666688	Transaldolase	35.75/34.74	6.4/7.7	*
Fermentation					
111	gi|295674635	Alcohol dehydrogenase	38.00/36.00	7.5/8.7	5.23E−03
114	gi|29566616	Alcohol dehydrogenase	44.83/35.00	8.9/8.0	3.16E−02
39	gi|295671230	Pyruvate decarboxylase	63.79/56.00	6.3/7.5	4.07E−02
Glyoxylate cycle					
57	gi|295664927	ATP-citrate-lyase	52.95/45.50	5.9/7.1	*
58	gi|295664927	ATP-citrate-lyase	52.95/47.00	5.9/7.0	1.25E−02
Methylcitrate cycle					
87	gi|295666179	2-methylcitrate synthase	51.51/44.00	9.0/9.3	4.21E−04
Metabolism					
Amino acid metabolism					
64	gi|295659992	Serine hydroxymethyltransferase	52.42/47.00	8.2/8.9	1.30E−04
8	gi|295659538	Methionine Cobalamin-independent synthase	87.30/83.40	6.2/8.2	*
106	gi|295673122	L-threonine 3-dehydrogenase	38.08/36.00	5.8/6.6	7.85E−03
101	gi|225678712	Ketol-acid reductoisomerase	44.86/38.00	9.1/8.0	1.01E−02
181	gi|226294753	1,2-dihydroxy-3-keto-5-methylthiopentene dioxygenase	20.90/19.10	5.5/6.1	1.12E−04
137	gi|295663891	2,5-diketo-D-gluconic acid reductase A	32.05/31.88	6.6/7.9	4.34E−09
151	gi|295665021	Chorismate mutase	38.05/28.00	8.4/6.0	1.08E−04
Nitrogen metabolism					
72	gi|295668479	Formamidase	46.15/45.40	6.1/7.2	*
Nucleotide metabolism					
32	gi|295672652	Bifunctional purine biosynthesis protein ADE17	67.21/60.94	6.7/8.5	*
96	gi|295674697	Adenosine kinase	36.61/37.00	5.4/5.8	3.85E−03
45	gi|295666938	Nucleoside diphosphate kinase	16.88/50.40	6.8/5.7	1.58E−04
190	gi|295658312	L-PSP endoribonuclease family protein (Hmf1)	18.72/14.00	8.9/6.5	1.52E−02
Cell rescue, defense and virulence					
Stress response					
18	gi|225681491	Hsp70-like protein	73.80/67.96	5.9/5.2	6.73E−04
13	gi|295659116	Hsp70-like protein	70.91/65.00	5.0/4.8	8.01E−04
79	gi|14538021	Heat shock protein 70	40.97/40.00	5.0/6.0	4.09E−02
2	gi|225679503	Heat shock protein SSB	67.26/82.43	5.3/4.8	4.76E−02
Detoxification					
40	gi|24528587	Peroxisomal Catalase	57.47/54.00	6.5/7.8	2.06E−03
176	gi|295669402	Mn superoxide dismutase	24.81/18.08	8.9/8.2	2.31E−04
175	gi|17980998	Y20 protein	21.64/17.10	6.0/7.2	*
62	gi|295664022	Glutathione reductase	51.95/47.00	6.7/8.5	5.57E−04
12	gi|295673162	Disulfide isomerase Pdi1	59.30/61.00	4.8/4.6	5.99E−03
Cell cycle and DNA processing					
123	gi|295661300	DNA damage checkpoint protein rad24	29.73/32.00	4.6/4.3	1.59E−03
162	gi|295666440	Sporulation-regulated protein	44.15/43.45	5.2/5.1	*
Protein fate					
156	gi|295674837	HAD-superfamily hydrolase	27.32/25.00	5.6/6.3	1.49E−02
120	gi|295661059	G-protein complex beta subunit CpcB	35.46/34.00	6.5/7.9	2.89E−02
184	gi|295672447	Peptidyl-prolyl cis–trans isomerase H	20.02/15.00	8.8/9.7	5.95E−03
183	gi|295672668	Peptidyl-prolyl cis–trans isomerase B	22.81/14.00	7.8/8.5	3.98E−03
Protein synthesis					
65	gi|295671178	Elongation factor 1-alpha	50.55/48.00	9.2/10.2	4.42E−03

(*continued on next page*)

Table 1 (*continued*)

Spot number[a]	Accession number[b]	Protein description	MW (kDa) Theo/Exp[c]	*p*I Theo/Exp[d]	*p*-value[e]
124	gi|295667868	Elongation factor 1-beta	25.93/32.00	4.7/4.6	6.90E−03
86	gi|295668925	Elongation factor 1-gamma 1	45.88/41.00	8.2/9.1	1.10E−02
Miscellaneous					
117	gi|225680961	Inorganic pyrophosphatase	51.79/34.00	8.1/4.9	5.69E−04
157	gi|295656848	TCTP family protein	20.28/21.00	4.7/4.5	6.13E−05
126	gi|226293104	Spermidine synthase	33.64/30.58	5.3/5.4	3.06E−02
89	gi|30351156	14-3-3-like protein	33.80/35.40	4.9/4.4	4.66E−02
53	gi|295665123	Aldehyde dehydrogenase	54.55/48.00	5.8/6.7	3.89E−05
Unclassified proteins					
80	gi|295674501	Conserved hypothetical protein	40.91/40.00	5.8/6.1	3.65E−04
125	gi|295660977	Conserved hypothetical protein	32.44/32.00	5.1/4.9	9.34E−03
185	gi|295658863	Conserved hypothetical protein	17.48/13.00	5.1/5.9	8.27E−04
187	gi|295672073	Hypothetical protein PAAG_01591	16.53/11.00	5.1/4.3	4.37E−04

[a] Spots were numbered according to Fig. 1.
[b] GenBank general information identifier. The accession number refers to higher scores on Mascot search.
[c] Experimental/theoretical molecular weight.
[d] Experimental/theoretical isoelectric point.
[e] $p \leqslant 0.05$ was considered statistically significant.
[*] Spots visualized only in *Pb*01.

test to compare the differences in protein expression among the four analyzed proteomes. According to ANOVA and Tukey's test, a total of 301 spots presented differential expression. At this step, the FDR correction for protein identification was estimated (values below 0.05%) and indicated the statistical significance of 267 spots, as depicted in Fig. S1. Those spots with over a 1.5-fold difference in their relative abundance among the four samples numbered 267, and those with a *p*-value equal to or less than 0.05 in ANOVA/Tukey's test were considered differentially expressed. The Coomassie G-250 blue-stained maps were used for the mass spectrometry identification of the individual protein spots. A total of 193 proteins/isoforms that were differentially expressed when comparing *Pb*01, *Pb*339, *Pb*2 and *Pb*EPM83 were unambiguously identified by PMF and confirmed by ion fragmentation. A summation of the analyzed spots is presented in Fig. S1.

Table S1 displays all of the proteins and isoforms, totaling 193, that were identified in the analysis. The list of identified proteins/isoforms and additional information, such as spot identification, GenBank general information identifiers (gi) and MS/MS mascot scores, are presented.

3.2. Abundantly detected proteins in Pb01, Pb2, Pb339 and PbEPM83

In this report, we describe the proteins that were differentially expressed in the cited members of the *Paracoccidioides* complex. The identified proteins were classified based on their main activity according to the Munich Information Center for Protein Sequences (MIPS) categorization, molecular weight and *p*I, theoretical and calculated, as well as the *p*-values associated with each spot comparison as depicted in Tables 1–4.

Some of the exclusively expressed proteins are related to basic processes found in virtually all organisms. To exclude the influence of differences in the protein predicted sequences in mass or *pI*, a sequence comparison was performed using the three genomes that were available for *Paracoccidioides*. The analysis revealed that the sequences are present as high sequence similarity among the investigated isolates and that the predicted *p*Is and masses are very similar among orthologous sequences.

When comparing the proteomes, from the 193 identified, 59 proteins/isoforms were preferentially expressed in *Pb*01, compared to *Pb*2, *Pb*339, and *Pb*EPM83, as depicted in Table 1. Most of the enzymes of the glycolysis pathway, represented by twelve isoforms corresponding to seven different proteins, were more abundant in *Pb*01 than in the other representatives of the genus *Paracoccidioides,* as depicted in Table 1. It is also noteworthy that the member of the phylogenetic species *Pb*01-*like* presented a high expression level of alcohol dehydrogenases, compared to the representatives of other phylogenetic species. In addition, pyruvate decarboxylase was over-expressed in this phylogenetic species. Considering nitrogen metabolism, an isoform of formamidase was highly induced in *Pb*01 compared to the representatives of other phylogenetic species. Additionally, some enzymes of amino acid metabolism, such as serine hydroxylmetyltransferase, methionine cobalamin independent synthase, L-threonine-3-dehydrogenase, and chorismate mutase, were up-regulated in *Pb*01, strongly suggesting that the biosynthesis of some amino acids, such as valine, methionine and tyrosine, could be over-regulated in this isolate (Table 1). Proteins of the detoxification pathways that are represented by peroxisomal catalase, Mn superoxide dismutase, Y20, glutathione reductase and disulfide isomerase presented isoforms with high expression in *Pb*01 compared to *Pb*339, *Pb*2 and *Pb*EPM83 (Table 1).

When comparing the proteome of *Pb*2 with those of *Pb*01, *Pb*339 and *Pb*EPM83, 53 proteins/isoforms were identified that were preferentially expressed by *Pb*2, as depicted in Table 2. The enzymes of the oxidative and non-oxidative reactions of the pentose-phosphate pathway were preferentially expressed in *Pb*2 compared to the other analyzed members of the genus *Paracoccidioides* as follows: transaldolase, 6-phosphogluconate dehydrogenase, 6-phosphogluconolactonase and transketolase were increased in *Pb*2 (Table 2). Notably, also in *Pb*2, similar to that observed in *Pb*01, the metabolism of amino acids seems to be over-regulated. The enzymes that are related to the biosynthesis of the branched chain amino acids lysine and methionine were over-accumulated in *Pb*2. Of special note, the production of fumarate and acetoacetyl CoA seems to be induced, as interpreted from the over-accumulation of the enzymes 4-hydroxyphenylpyruvate dixoygenase and fumarylacetoacetase, both involved in the degradation of tyrosine and phenylalanine (Table 2). Cellular detoxification enzymes, such as peroxisomal catalase, Cu and Zn superoxide dismutase and 2-alkenal reductase, were also induced in *Pb*2 (Table 2).

When comparing the proteome of *Pb*339 with the other proteomes, 43 proteins/isoforms were preferentially expressed. β-oxidation enzymes, such as acyl CoA dehydrogenase, 3-hydroxybutyryl CoA dehydrogenase and enoyl-CoA hydratase were up-regulated

Table 2
Proteins/isoforms with increased abundance in *Pb*2.

Spot number[a]	Accession number[b]	Protein description	MW (kDa) Theo/Exp[c]	*p*I Theo/Exp[d]	*p*-value[e]
Energy					
Glycolysis and gluconeogenesis					
30	gi|295658778	Phosphoenolpyruvate carboxykinase	63.89/58.00	6.1/7.2	1.08E−03
27	gi|295658778	Phosphoenolpyruvate carboxykinase	63.89/59.00	6.1/7.3	1.44E−02
Tricarboxylic-acid pathway					
129	gi|295673937	Malate dehydrogenase	36.02/33.00	8.9/7.8	5.10E−04
9	gi|226293399	Aconitase	82.47/79.00	7.0/8.1	4.69E−04
56	gi|226294995	Dihydrolipoyl dehydrogenase	55.40/47.00	8.0/7.6	3.24E−04
61	gi|295668473	Dihydrolipoyl dehydrogenase	56.06/47.00	8.2/7.8	1.37E−03
85	gi|295658897	Citrate synthase	52.20/43.00	8.7/8.4	4.84E−03
Pentose-phosphate pathway					
119	gi|225683456	Transaldolase	35.86/34.50	6.1/7.3	3.93E−06
51	gi|226292147	6-phosphogluconate dehydrogenase	54.60/44.50	5.7/6.6	9.55E−08
152	gi|225677822	6-phosphogluconolactonase	29.30/27.90	5.8/7.1	9.15E−06
24	gi|295665967	Transketolase	74.94/63.40	5.9/7.3	2.97E−06
Fermentation					
163	gi|295674635	Alcohol dehydrogenase	38.00/35.60	7.5/9.0	6.01E−04
Glyoxylate cycle					
33	gi|295660969	Isocitrate lyase	60.17/56.00	6.7/7.6	2.29E−03
Methylcitrate cycle					
31	gi|295666177	Mitochondrial 2-methylisocitrate lyase	67.25/60.00	8.7/8.3	8.60E−03
Metabolism					
C-compound and carbohydrate metabolism					
29	gi|225678915	1,4-alpha-glucan-branching enzyme	80.30/66.20	5.7/6.8	5.36E−04
100	gi|295662360	Mannitol-1-phosphate 5-dehydrogenase	43.11/39.00	5.6/6.5	2.00E−03
Amino acid metabolism					
70	gi|226289087	Argininosuccinate synthase	46.80/45.00	5.4/5.7	1.78E−03
44	gi|295660644	Argininosuccinate synthase	46.76/46.00	5.1/5.2	1.25E−03
7	gi|295659538	Methionine Cobalamin-independent synthase	87.30/83.00	6.2/7.9	2.16E−02
28	gi|295663883	Dihydroxy-acid dehydratase	65.40/61.00	6.0/6.9	2.20E−02
105	gi|295658704	4-hydroxyphenylpyruvate dioxygenase	45.67/38.00	5.5/6.5	8.85E−03
74	gi|225682808	Adenosylhomocysteinase	49.00/42.70	5.8/6.9	7.42E−04
76	gi|295669670	Adenosylhomocysteinase	49.02/43.00	5.8/6.8	5.52E−04
99	gi|225685311	Saccharopine dehydrogenase	42.10/41.00	5.8/6.7	2.23E−06
82	gi|226288132	Fumarylacetoacetase	46.70/42.30	6.1/7.2	1.67E−06
Sulfur metabolism					
43	gi|225679471	Sulfite oxidase	48.90/48.40	5.1/5.3	4.18E−06
Nucleotide Metabolism					
164	gi|225678337	Adenosine kinase	39.00/36.80	6.0/5.9	1.59E−03
63	gi|295664573	Adenylosuccinate lyase	54.90/49.00	7.1/8.6	8.99E−04
Cell rescue, defense and virulence					
Detoxification					
41	gi|225681400	Peroxisomal catalase	57.65/53.00	6.4/7.9	6.54E−04
188	gi|295666684	Cu, Zn superoxide dismutase	15.97/11.00	5.9/7.1	4.20E−03
113	gi|295664270	2-alkenal reductase	38.64/37.00	8.7/9.7	1.75E−02
Cell cycle and dna processing					
112	gi|225681947	UDP-galactopyranose mutase	59.60/50.10	6.5/7.6	1.92E−04
Protein fate					
139	gi|225682490	G-protein complex beta subunit CpcB	35.40/34.20	6.5/8.0	1.14E−04
154	gi|226290547	HAD-superfamily hydrolase	27.30/27.20	5.4/5.8	7.94E−03
78	gi|295668481	Peptidyl-prolyl cis–trans isomerase D	41.36/40.00	5.3/5.5	8.59E−04
135	gi|225679389	Ubiquitin-conjugating enzyme	28.50/30.40	4.9/4.7	2.26E−07
143	gi|225684267	Ubiquitin carboxyl-terminal hydrolase	27.20/27.80	4.8/4.4	5.96E−04
3	gi|225679863	Aminopeptidase	109.4/82.00	6.3/5.6	2.13E−03
4	gi|226295047	Puromycin-sensitive aminopeptidase	102.6/80.10	6.7/5.9	5.62E−07
14	gi|225685107	Beta-Ala-His dipeptidase	53.50/48.50	5.3/5.7	1.87E−02
Protein synthesis					
178	gi|295657799	40S ribosomal protein S12	16.87/16.00	5.0/4.6	1.02E−04
84	gi|225678523	Elongation factor 1-gamma 1	45.90/41.00	7.6/8.5	1.03E−04
131	gi|225679636	Translation elongation factor eEF-1 beta chain	26.40/31.90	4.6/4.4	3.07E−05
20	gi|225685037	Glycyl-tRNA synthetase	74.80/64.00	5.7/6.4	8.28E−06
46	gi|225685085	Seryl-tRNA synthetase	55.20/51.40	5.5/7.0	1.03E−02

(*continued on next page*)

Table 2 (*continued*)

Spot number[a]	Accession number[b]	Protein description	MW (kDa) Theo/Exp[c]	*p*I Theo/Exp[d]	*p*-value[e]
Cellular transport, transport facilities and transport routes					
169	gi|295666381	GTP-binding nuclear protein GSP1/Ran	24.08/22.00	6.9/7.8	5.91E−03
Miscellaneous					
81	gi|295669073	12-oxophytodienoate reductase	43.24/41.90	8.6/6.9	5.72E−04
97	gi|295659136	Coproporphyrinogen III oxidase	51.97/41.00	6.6/6.4	2.51E−03
186	gi|225678115	Peroxisomal matrix protein	18.00/16.80	5.6/6.3	2.14E−02
180	gi|225678502	Decarboxylase family protein	27.40/27.10	5.6/6.0	1.54E−02
Unclassified proteins					
133	gi|225681437	Conserved hypothetical protein	31.80/31.90	5.7/6.5	4.16E−04
193	gi|226294299	Conserved hypothetical protein	14.90/13.60	10.0/10.3	2.25E−04
94	gi|295668298	Conserved hypothetical protein	34.72/37.00	5.3/5.2	2.45E−03

* Spots visualized only in *Pb*2.
[a] Spots were numbered according to Fig. 1.
[b] GenBank general information identifier. The accession number refers to higher scores on Mascot search.
[c] Experimental/theoretical molecular weight.
[d] Experimental/theoretical isoelectric point.
[e] $p \leqslant 0.05$ was considered statistically significant.

(Table 3). The proteins that were involved in mitochondrial electron transport, such as ATP synthase, were more abundantly expressed in this isolate. Some isoforms of enzymes that were related to cellular detoxification, such as Mn superoxide dismutase and mitochondrial peroxiredoxin PRX1, were up-regulated in *Pb*339 compared to *Pb*01, *Pb*2 and *Pb*EPM83. The 27 kDa antigenic protein presented a higher level of expression in *Pb*339 (Table 3).

When comparing the other proteomes to that of *Pb*EPM83, a member of the PS3 clade, 38 proteins were preferentially expressed. The isoforms of proteins that were related to the heat shock response were more abundant in *Pb*EPM83, as depicted in Table 4. The isoforms of enzymes of the glycolysis and TCA cycles were also abundantly expressed in this isolate. The antigenic protein GP43 also presented a higher level of expression in *Pb*EPM83.

Pie charts representing the distribution of the identified differential spots of each isolate, according to their biological functions, are shown in Fig. S2.

3.3. Proteomic variation among members of the Paracoccidioides genus

The proteins/isoforms exhibiting significantly altered expression in the analyzed isolates entered into the Multi Experiment Viewer software V.4.8 (www.tm4.org/mev/) for hierarchical clustering as depicted in Fig. S3. The clustered data demonstrated a clear pattern of proteomic diversity and provided clear and detailed information regarding the cellular processes that were represented more in one *Paracoccidioides* isolate compared to the other three analyzed. As observed, several groups of proteins/isoforms representing different metabolic processes with differences in spots intensities were found. The general pattern evidenced by the hierarchical clustering indicated a differential protein profile among the analyzed members of the *Paracoccidioides* genus.

3.4. A comparative analysis of the most induced metabolic pathways in members of Paracoccidioides complex, as revealed by proteomic analysis

The abundance of the different protein categories revealed the plausible metabolic/physiological strategies used by each member of the *Paracoccidioides* genus. Six main strategies were established according to the proteomic data: (i) glycolysis and alcoholic fermentation; (ii) TCA cycle; (iii) pentose phosphate pathway; (iv) β-oxidation; (v) heat shock response; and (vi) reactive oxygen species (ROS) scavenging, as depicted in Fig. 2. Although the experiments were performed in a complex medium, the differential proteomic profile among *Paracoccidioides* cryptic species has evidenced specific metabolic profiles for each species. *Pb*01 seems to use glycolysis preferentially via the anaerobic pathway, producing ethanol, as suggested by the presence of seven induced glycolytic enzymes and the enzymes pyruvate decarboxylase and alcohol dehydrogenase. Notably, proteins related to the detoxification response were also up-regulated, possibly to counteract the reactive oxygen species in *Pb*01.

*Pb*2 presents a high number of enzymes that are related to the metabolism of amino acids such as lysine, tyrosine, cysteine and methionine. In particular, this isolate seems to obtain fumarate and acetoacetyl CoA by the degradation of the amino acids phenylalanine and tyrosine to supply the Krebs cycle, which is up-regulated in this isolate, indicating that the member of the cryptic species *PS*2 can preferentially degrade amino acids to obtain energy by the TCA aerobically. The enzymes of the pentose phosphate pathway were induced in *Pb*2, putatively producing NADPH for biosynthetic processes and/or to degrade the reactive oxygen species that are produced by aerobic metabolism, as indicated by the up-regulation of the detoxification enzyme isoforms peroxisomal catalase and Cu and Zn superoxide dismutase.

In contrast, the isolate *Pb*339 seems to metabolically favor the degradation of lipids by beta-oxidation, as depicted by the increased levels of the enzymes enoyl-CoA hydratase, short chain-specific acyl-CoA dehydrogenase and 3-hydroxyisobutyryl-CoA hydrolase. In addition, the levels of ATP synthase subunits increased in *Pb*339, indicating a preferential aerobic degradation of fatty acids to yield energy.

Regarding *Pb*EPM83, the comparative proteomic analysis indicates that this isolate presents a preferential aerobic degradation of glucose-related molecules, as depicted by the up-regulation of some glycolytic and TCA cycle-related enzymes. Interestingly, the induction of several heat shock proteins in *Pb*EPM83 could be attributed to a pronounced heat shock response in this member of the phylogenetic species *PS*3.

3.5. Biochemical confirmatory assays

To validate the significance of the proteomic results, biochemical assays were performed. The intracellular ethanol was higher in *Pb*01 after 48 h of culture growth, as depicted in Fig. 3A, indicating increased alcoholic fermentation compared to the other isolates. Additionally, the activity of the enzyme formamidase increased in *Pb*01 (Fig. 3B), confirming the proteomic data in which an

Table 3
Proteins/isoforms with increased abundance in *Pb*339.

Spot number[a]	Accession number[b]	Protein description	MW (kDa) Theo/Exp[c]	*p*I Theo/Exp[d]	*p*-value[e]
Energy					
Glycolysis and gluconeogenesis					
49	gi|146762537	Enolase	47.41/45.00	5.6/6.0	1.15E−04
47	gi|226290885	Glyceraldehyde-3-phosphate dehydrogenase	36.57/33.30	7.1/8.3	*
Tricarboxylic-acid pathway					
88	gi|295658595	Pyruvate dehydrogenase E1 component subunit alpha	45.31/40.20	8.62/7.7	*
Oxidation of fatty acids					
153	gi|226289575	Enoyl-CoA hydratase	31.57/25.11	8.8/8.7	1.92E−05
158	gi|225677560	Short-chain specific acyl-CoA dehydrogenase	47.81/39.14	8.2/5.6	2.48E−10
38	gi|295670601	3-hydroxyisobutyryl-CoA hydrolase	57.35/50.94	7.0/6.5	1.78E−05
Electron transport and membrane-associated energy conservation					
77	gi|295658821	ATP synthase subunit beta	55.18/40.20	5.2/4.6	*
42	gi|295658821	ATP synthase subunit beta	55.18/47.00	5.2/4.7	5.62E−03
34	gi|226287911	ATP synthase subunit beta	55.24/51.20	5.3/4.4	3.98E−05
Metabolism					
C-compound and carbohydrate metabolism					
149	gi|295666718	Sorbitol utilization protein SOU2	31.48/30.00	7.0/8.2	1.17E−04
Amino acid metabolism					
5	gi|226291641	3-isopropylmalate dehydratase	85.11/79.03	5.8/6.9	*
95	gi|225677671	3-isopropylmalate dehydrogenase	38.91/37.90	5.3/5.4	*
Nitrogen metabolism					
55	gi|225678657	Formamidase	46.08/43.60	6.0/7.0	*
174	gi|295658559	Nitroreductase family protein	25.26/22.60	6.2/7.8	1.48E−04
Nucleotide metabolism					
23	gi|226292595	Bifunctional purine biosynthesis protein ADE17	69.40/58.16	7.2/8.2	*
Cell rescue, defense and virulence					
Stress response					
16	gi|295659837	Heat shock protein SSB1	60.69/64.00	5.4/5.2	7.25E−06
170	gi|225680288	Wos2	23.62/26.61	4.3/3.8	1.04E−02
11	gi|225678945	Clock-controlled gene-9 protein	81.88/69.60	6.0/7.2	*
Detoxification					
172	gi|225682872	Mn superoxide dismutase	23.81/21.95	7.0/8.2	*
177	gi|225682872	Mn superoxide dismutase	23.81/22.31	7.0/8.4	*
166	gi|226291569	Mitochondrial peroxiredoxin PRX1	24.90/24.30	5.2/5.1	5.02E−05
160	gi|295668244	Mitochondrial peroxiredoxin PRX1	24.88/22.00	5.2/5.1	6.42E−04
Cell cycle and DNA processing					
1	gi|295664474	Cell division cycle protein	90.50/91.30	4.9/5.1	6.16E−09
73	gi|295668877	Actin	41.82/41.00	5.6/6.0	2.73E−04
68	gi|295672568	ATP-dependent RNA helicase eIF4A	45.00/42.70	5.1/5.1	1.03E−02
Protein fate					
132	gi|226292478	Proteasome component C1	32.80/31.40	5.1/5.2	7.98E−04
159	gi|225680770	Proteasome subunit beta type-1-A	29.20/27.40	6.1/5.1	*
136	gi|225678501	Proteasome subunit alpha type-1 Pb03	29.00/27.88	5.2/5.1	6.18E−06
189	gi|295662699	Peptidyl-prolyl cis–trans isomerase cypE	17.52/12.00	6.0/7.3	5.85E−04
37	gi|226294989	Peptidyl-prolyl cis–trans isomerase D	41.27/48.15	5.4/5.6	9.90E−07
171	gi|225684870	V Chain V	21.63/21.46	6.0/7.0	*
36	gi|225681422	Kynureninase	54.19/49.24	5.3/5.5	2.07E−07
75	gi|226292231	Prolyl peptidase	51.19/41.40	5.5/6.4	7.68E−05
Protein synthesis					
130	gi|226289773	40S ribosomal protein S3	29.80/40.80	8.9/8.5	1.20E−07
93	gi|295671352	40S ribosomal protein S0	32.07/37.00	4.8/4.7	1.50E−03
Antigenics proteins					
168	gi|1778408	27 kDa antigen, partial	24.71/23.13	8.8/8.6	2.42E−13
167	gi|1778408	27 kDa antigen, partial	24.71/23.13	8.8/8.2	6.43E−06
Miscellaneous					
102	gi|295669073	12-oxophytodienoate reductase	43.24/40.48	8.6/9.3	2.43E−03
103	gi|295669073	12-oxophytodienoate reductase	43.24/40.00	8.6/9.5	1.54E−02
148	gi|226294448	Nicotinate-nucleotide pyrophosphorylase	33.85/27.68	6.5/7.8	1.02E−10
54	gi|225680265	Aldehyde dehydrogenase	54.69/44.80	5.9/6.6	8.31E−06

(*continued on next page*)

Table 3 (*continued*)

Spot number[a]	Accession number[b]	Protein description	MW (kDa) Theo/Exp[c]	*p*I Theo/Exp[d]	*p*-value[e]
Unclassified proteins					
191	gi|225681129	Predicted protein	13.46/11.64	5.7/6.5	*
182	gi|225678257	Conserved hypothetical protein	19.20/19.70	8.6/9.7	2.35E−02

[a] Spots were numbered according to Fig. 1.
[b] GenBank general information identifier. The accession number refers to higher scores on Mascot search.
[c] Experimental/theoretical molecular weight.
[d] Experimental/theoretical isoelectric point.
[e] $p \leqslant 0.05$ was considered statistically significant.
* Spots visualized only in *Pb*339.

Table 4
Proteins/isoforms with increased abundance in *Pb*EPM83.

Spot number[a]	Accession number[b]	Protein description Theo/Exp[c]	MW (kDa)	*p*I Theo/Exp[d]	*p*-value[e]
ENERGY					
Glycolysis and gluconeogenesis					
116	gi|225682647	Fructose-1,6-bisphosphatase	38.90/38.00	5.8/6.3	1.02E−04
107	gi|295671120	Fructose-bisphosphate aldolase	39.70/37.50	6.0/7.4	1.78E−05
98	gi|295669690	Phosphoglycerate kinase	45.31/42.10	6.4/7.4	1.32E−04
Tricarboxylic-acid pathway					
140	gi|295673937	Malate dehydrogenase	36.02/29.30	8.9/9.4	6.66E−03
118	gi|239609129	Pyruvate dehydrogenase E1 component subunit beta	41.28/30.20	7.5/5.5	*
138	gi|225683092	Pyruvate dehydrogenase E1 component subunit alpha	40.99/32.65	8.1/5.7	6.09E−04
144	gi|225684846	Fumarate hydratase	60.70/42.45	9.0/8.3	8.39E−06
69	gi|225683829	Citrate synthase	51.60/43.40	9.0/5.4	7.93E−04
92	gi|295658897	Citrate synthase	52.20/40.54	8.7/8.7	6.39E−05
Methylcitrate cycle					
59	gi|295666197	2-methylcitrate dehydratase	62.26/59.00	8.5/7.7	2.79E−07
Metabolism					
C-compound and carbohydrate metabolism					
147	gi|225678580	Polysaccharide deacetylase family protein	36.20/35.90	5.8/7.2	2.51E−3
Amino acid metabolism					
66	gi|225560729	Serine hydroxymethyltransferase	52.30/46.00	8.5/9.2	4.65E−03
146	gi|225683962	Anthranilate synthase component 1	58.09/52.30	5.6/6.1	3.99E−03
Cell rescue, defense and virulence					
Stress response					
6	gi|60656557	Heat shock protein 90	80.32/78.00	4.9/4.9	1.41E−04
17	gi|295671569	Heat shock protein SSC1	73.82/66.00	5.9/5.4	3.82E−04
10	gi|295673716	Hsp70-like protein	68.86/62.85	5.3/4.7	1.88E−04
71	gi|4164594	Heat shock protein 70	65.28/41.94	5.4/5.4	3.08E−10
22	gi|295663681	Heat shock protein 90	78.65/57.44	4.9/4.8	1.19E−02
15	gi|295663681	Heat shock protein 90	78.64/62.00	4.9/4.8	4.06E−04
35	gi|295658865	Heat shock protein 60	62.26/54.00	5.5/5.1	2.42E−04
Cell cycle and DNA processing					
60	gi|225681947	UDP-galactopyranose mutase	59.60/47.90	6.5/7.4	6.76E−06
Protein fate					
127	gi|225680783	Proteasome subunit alpha type-3	29.70/32.40	5.2/5.3	7.17E−04
173	gi|225679093	Proteasome subunit alpha type-4	28.10/24.70	5.7/6.3	9.30E−05
145	gi|225684609	Proteasome subunit alpha type-2	26.97/25.52	5.3/6.6	1.28E−03
150	gi|295672968	Phosphomannomutase	30.57/27.00	5.6/5.8	2.43E−05
141	gi|226289845	Gamma-glutamyltranspeptidase	64.08/40.2	5.9/7.1	1.58E−03
Protein synthesis					
19	gi|225682377	Phenylalanyl-tRNA synthetase beta chain	68.60/62.00	5.6/6.1	1.80E−04
Cellular transport, transport facilities and transport routes					
67	gi|295662102	Rab GDP-dissociation inhibitor	52.53/48.45	5.4/10.4	*
Antigenics proteins					
90	gi|8576322	43 kDa secreted glycoprotein precursor	46.28/39.19	6.8/8.1	6.34E−07
91	gi|8576322	43 kDa secreted glycoprotein precursor	46.28/39.35	6.8/7.3	1.33E−02

Table 4 (*continued*)

Spot number[a]	Accession number[b]	Protein description Theo/Exp[c]	MW (kDa)	*p*I Theo/Exp[d]	*p*-value[e]
Miscellaneous					
104	gi|225678587	12-oxophytodienoate reductase	43.00/40.5	8.5/9.4	2.18E−06
134	gi|225683930	Hydrolase	50.50/31.40	9.7/8.8	2.34E−03
128	gi|225685013	Pyridoxine biosynthesis protein PDX1	34.42/33.47	6.0/6.6	3.89E−04
179	gi|226287294	4-carboxymuconolactone decarboxylase family protein	20.90/21.50	5.3/5.6	2.75E−03
Unclassified proteins					
165	gi|295666522	Conserved hypothetical protein	21.15/20.00	5.1/5.0	2.11E−04
142	gi|226295016	Conserved hypothetical protein	34.78/34.50	4.5/3.5	4.78E−05
192	gi|226294299	Conserved hypothetical protein	14.92/12.60	10.0/9.3	1.98E−03
155	gi|225678961	Predicted protein	24.60/23.30	8.4/8.7	1.23E−07

[a] Spots were numbered according to Fig. 1.
[b] GenBank general information identifier. The accession number refers to higher scores on Mascot search.
[c] Experimental/theoretical molecular weight.
[d] Experimental/theoretical isoelectric point.
[e] $p \leqslant 0.05$ was considered statistically significant.
[*] Spots visualized only in *Pb*EPM83.

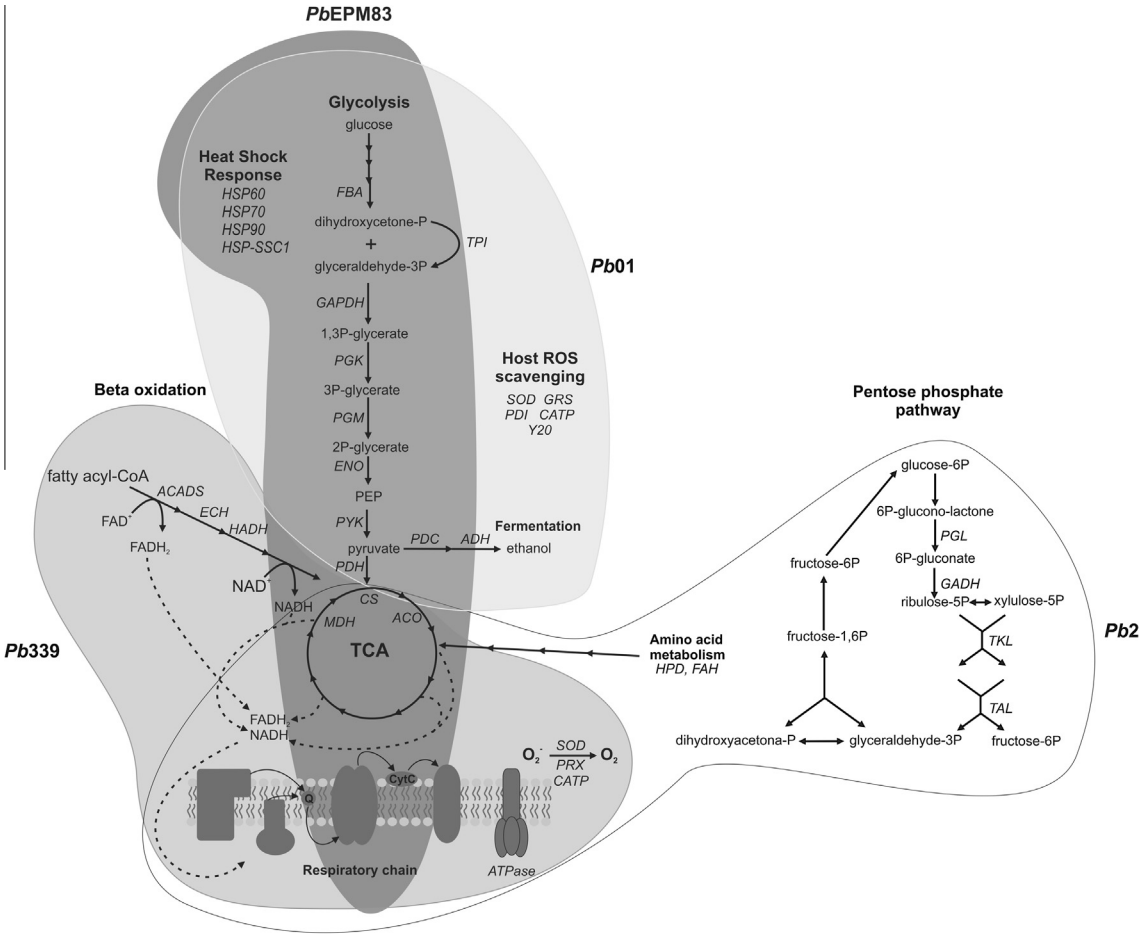

Fig. 2. Metabolic features of *Paracoccidioides* phylogenetic species identified by proteomic analysis. The pathways were constructed based on the preferential identification of proteins in each *Paracoccidioides* isolate. In the glycolytic pathway, the up-regulated proteins/isoforms were those that were related to the following enzymes: FBA (Fructose 1,6-biphosphate aldolase 1), TPI (Triosephosphate isomerase), GAPDH (Glyceraldehyde-3-phosphate dehydrogenase), PGK (Phosphoglycerate kinase), PGM (2,3-bisphosphoglycerate-independent phosphoglyceratemutase), ENO (Enolase) and PYK (Pyruvate kinase). The enzymes PDC (Pyruvate decarboxylase) and ADH (Alcohol dehydrogenase) are induced enzymes related to ethanol production through fermentation. The beta-oxidation-induced proteins/isoforms were ACADS (Short chain-specific acyl-CoA dehydrogenase), ECH (Enoyl-CoA hydratase) and 3-hydroxybutyryl-CoA dehydrogenase (HADH). The over-expressed proteins/isoforms of the tricarboxylic acid pathway were PDH (Pyruvate dehydrogenase), CS (Citrate synthase), ACO (Aconitase) and MDH (Malate dehydrogenase). The amino acid metabolism enzymes were 4-hydroxyphenylpyruvate dioxygenase (HPD) and fumarylacetocatase (FAH). The ATP synthase subunit beta (ATPase) was identified. The over-regulated proteins/isoforms of the pentose phosphate pathway were PGL (6-phosphogluconolactonase), GADH (6-phosphogluconate dehydrogenase), TKL (Transketolase) and TAL (Transaldolase). The detoxification enzymes were SOD (Mn superoxide dismutase), PRX (Mitochondrial peroxiredoxin), CATP (Peroxisomal catalase), GRS (Glutathione reductase), PDI (Disulfide isomerase) and Y20 (flavodoxin-like protein). The over-regulated heat shock response proteins in *Pb*EPM83 were HSP60 (Heat shock protein 60), HSP70 (Heat shock protein 70), three isoforms of HSP90 (Heat shock protein 90) and HSP-SSC1 (Heat shock protein SSC1).

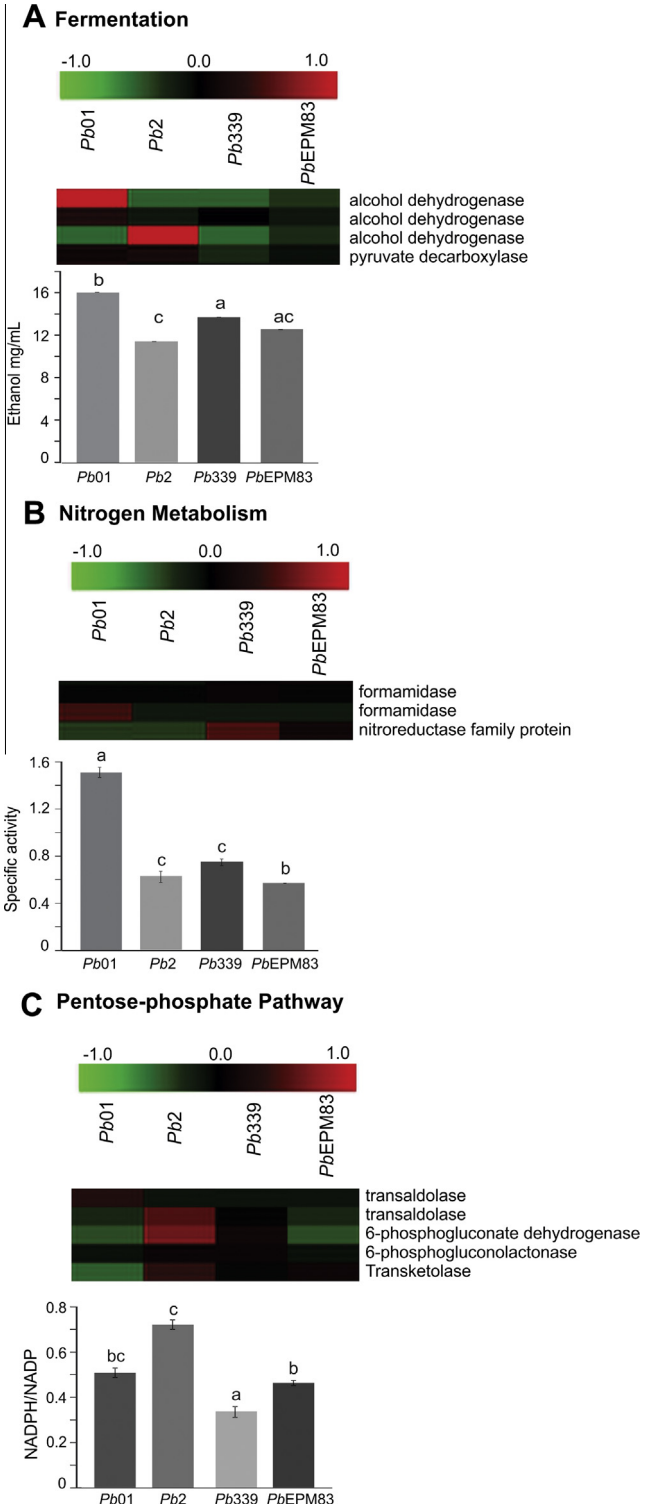

Fig. 3. Validation of proteomic data by enzymatic activity assays. (A) Determination of ethanol in yeast cells. The yeast cells were disrupted in the bead beater to determine the intracellular ethanol concentrations that were quantified using the UV-test Kit for ethanol, (R-Biopharm, Darmstadt, Germany). (B) The formamidase activity was measured by monitoring ammonia formation. The formamidase-specific activity was defined as the amount of enzyme required to hydrolyze 1 μmol formamide per minute per mg total protein. (C) Measurement of the intracellular NADPH/NADP$^+$ ratio in yeast cells. Using the NADP/NADPH Assay Kit (Abcam, Cambridge, UK) according to the manufacturer's instructions, we measured the intracellular NADP + and NADPH concentrations. The error bars indicate the standard deviations from three independent experiments that were performed in triplicate. The data were analyzed by a two-way ANOVA and Tukey's multiple comparison. The letters indicate the significant differences in the expression between samples.

isoform of this enzyme presented a 5.17-fold increase compared to the other isolates. In agreement with the increased expression of the enzymes of the pentose phosphate pathway in *Pb*2, the NADPH/NADP + ratio increased, as depicted in Fig. 3C.

In our proteomic analyses, the enzymes that were related to the inactivation of ROS were more highly expressed in *Pb*01, *Pb*2 and *Pb*339 than in P*b*EPM83. In tests using menadione as an oxidative stressor, *Pb*EPM83 depicted a higher susceptibility than the other isolates, corroborating the proteomic data (Fig. 4A).

The proteomic data also indicated that the isolate *Pb*2 depicted a low number of over-expressed heat shock proteins compared to the other isolates. Regarding the resistance to the heat shock, the different isolates of *Paracoccidioides* respond to a shift from 36 °C to 42 °C with a decrease in CFU counts. The results obtained for the heat shock analysis are presented in Fig. 4B, depicting a higher sensitivity of the isolate *Pb*2 to the temperature increase.

Additionally, the comparative proteomic data suggest that the representatives of the phylogenetic species of *Paracoccidioides* could establish different metabolic pathways by using different sources of carbon. In this sense, *Pb*339 seems to metabolically favor the degradation of lipids by beta-oxidation. Growth assays performed in the presence of oleic acid demonstrated that the isolate *Pb*339 can use oleic acid as an alternative carbon source (Fig. 4C).

4. Discussion

Metabolic and adaptive strategies comparing members of the *Paracoccidioides* genus have been discussed at the molecular level with genomic analyses (Desjardins et al., 2011). Nevertheless, these strategies have not been discussed in the light of experimental proteomic data until now. In the present study, we show how the proteins that are accumulated by an organism can indicate the physiological state of the cells. The comparative proteome profiles of *Pb*01, *Pb*2, *Pb*339 and *Pb*EPM83 are described here for the first time. Using a proteomic analysis, from a total of 714 detected spots, 343 were analyzed, and, from those, 193 were differentially expressed proteins/isoforms. The proteomic data demonstrated significant differences in the protein expression profiles among the representatives of different phylogenetic clades of the genus *Paracoccidioides*. The hierarchical clustering of the proteome profiles of the four isolates of *Paracoccidioides* reflect the phylogenetic relationships between these *Paracoccidioides* species, where S1 is considered an independent species, and *PS*3 is phylogenetically closer to *S*1 than to *PS*2. *Pb*01 is highly divergent from all other phylogenetic species (Matute et al., 2006; Teixeira et al., 2009).

Proteomes can give hints as to the physiological state of the cells. In our proteomic analysis, the expression levels of the enzymes that are related to glycolysis suggest the use of a more anaerobic metabolism for energy production from glucose in the *Pb*01 isolate. The high level of enzymes involved in glycolysis and alcoholic fermentation led to the assumption that this isolate could have a more anaerobic metabolism than do the others. The levels of ethanol were determined in the yeast cells of the analyzed isolates. As observed, the level of ethanol was higher in *Pb*01, corroborating a more anaerobic metabolism. Transcriptional studies have suggested a more anaerobic metabolism at the yeast phase of isolate *Pb*01, that could produce more ethanol compared to mycelia (Felipe et al., 2005). Consistent with these results, the proteomic analysis detected the accumulation of enzymes of the glycolysis pathway and of alcoholic fermentation at the transition from mycelium to yeast cells in *Pb*01 (Rezende et al., 2011). Studies had indicated the relevance of ethanol fermentation for pathogenic fungi. Proteomic studies suggest that ethanol fermentation contributes to the generation of energy in the conidia at dormancy or at the beginning of the germination process in *Aspergillus*

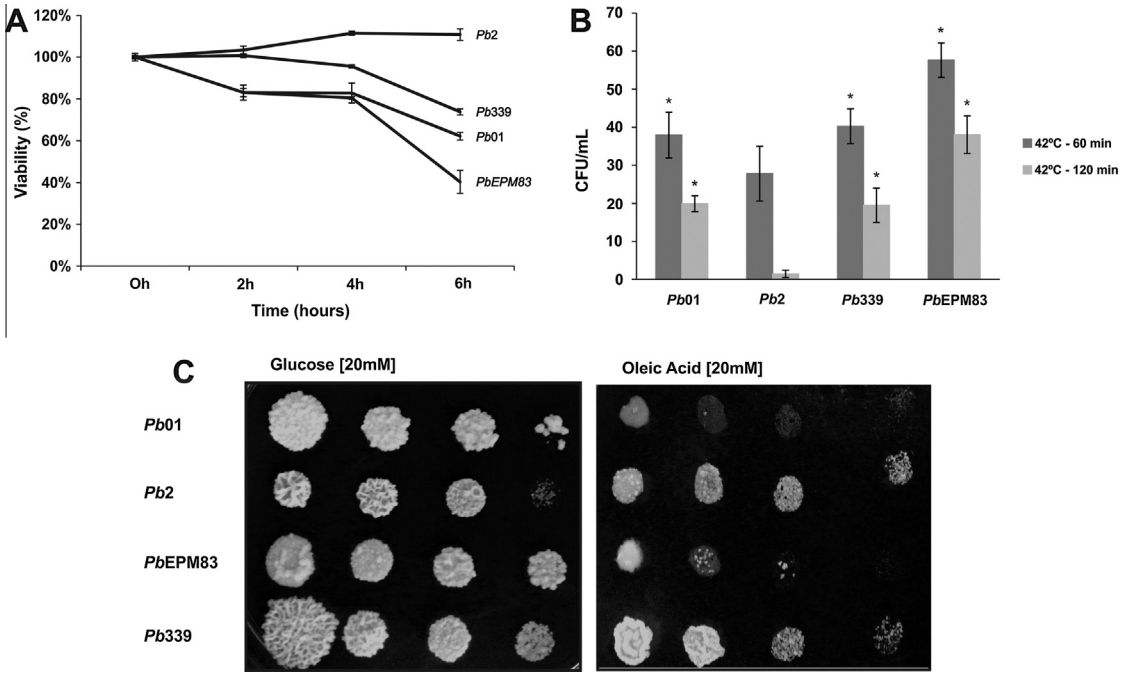

Fig. 4. Cell viability in the presence of oxidative stress, effect of heat shock on the viability of *Paracoccidioides* yeast cells and use of different carbon sources by isolates of *Paracoccidioides*. (A) The oxidative stress response was investigated in yeast cells of *Paracoccidioides* that were exposed to 1 mM menadione (Sigma Aldrich, Co) for 2, 4 and 6 h. The viability was determined by a membrane integrity analysis using propidium iodide (1 mg/mL) as a dead cell marker in a C6 Accuri flow cytometer (Accuri Cytometers, Ann Arbor, MI, USA). The experiments were performed in triplicate. Statistical analyses compared *Pb*EPM83 with the other isolates in this study and were performed by using Student's *t*-test; all of the samples showed *p*-values < 0.05 (*) and were considered statistically significant. The errors bars represent the standard deviation of three biological replicates. (B) Colony-forming units recovered from the plating of 10^2 viable cells in BHI semisolid medium after incubation under different conditions (36 °C, 42 °C/60 min and 42 °C/120 min), as determined after 7 days. The assay was performed in three independents replicates. Student's *t*-test was used for statistical comparisons of *Pb*2 with *Pb*01, *Pb*EPM83 and *Pb*339, and the observed differences were statistically significant ($p < 0.05^*$). The errors bars represent the standard deviation of three biological replicates. (C) The *Pb*01 (*01-like*), *Pb*2 (*PS2*), *Pb*339(*S1*) and *Pb*EPM83 (*PS3*) isolates were grown at 37 °C in Fava Netto's liquid medium under gentle shaking for 72 h. The cultures were serially diluted, and each dilution was spotted onto minimal medium containing different carbon sources (glucose and oleic acid) at 20 mM. The plates were incubated for 7 to 15 days at 37 °C.

fumigatus (Teutschbein et al., 2010). In addition, under hypoxic conditions, this fungus prioritizes the activation of ethanol fermentation (Barker et al., 2012).

The most induced metabolic strategies in *Pb*2 seem to be the pentose phosphate pathway, as revealed by comparative proteomics and confirmed by biochemical analysis. The induction of the non-oxidative branch of the pentose phosphate pathway can provide substrates for glycolysis. Additionally, the high expression of the enzymes of the oxidative branch can provide NADPH for use in biosynthetic processes (Rui et al., 2010). The degradation of amino acids that provide substrates for the TCA cycle is also a differential aspect of the metabolism of *Pb*2, as revealed by proteomic analysis. A striking feature of *Pb*339 is beta-oxidation. Growth assays in the presence of oleic acid corroborated the proteomic data. The oxidation of fatty acids is important for the utilization of storage lipids or exogenous fatty acids to generate acetyl coenzyme A (acetyl-CoA) for central carbon metabolism. The transcriptional profiling of *Cryptococcus neoformans* revealed that genes for peroxisomal-oxidation, fatty acid import, and lipid degradation were upregulated upon pathogen internalization and during pulmonary infection, suggesting that fatty acid metabolism may be important for the virulence of *C. neoformans* in mammals (Kretschmer et al., 2012). If this metabolic aspect can influence the virulence of *Pb*339, it should be a focus of future investigations. Compared to the other isolates, *Pb*EPM83 seems to preferentially utilize aerobic routes for energy production through carbohydrates, as suggested by the over-accumulation of glycolytic and TCA enzymes.

Protein metabolism appears to be central to growth in the Onygenales. Metabolic assays of the non-pathogenic Onygenales *Uncinocarpus reesiiu* demonstrated extensive growth on a wide range of proteinaceous substrates compared to carbohydrates (Desjardins et al., 2011). The metabolism of amino acids seems to be particularly relevant in *Pb*01 and *Pb*2 isolates compared to *Pb*339 and *Pb*EPM83. Whether this metabolic feature provides more attributes to an animal pathogen remains to be elucidated.

Enzymes that are related to the oxidative stress response were more abundant in *Pb*01, *Pb*2 and *Pb*339 compared to *Pb*EPM83, indicating a better response to reactive oxygen species (ROS) in these members of the *Paracoccidioides* complex. The human pathogenic fungi rely on mechanisms for protection against oxidative damage to defend against ROS that are released by host cells in the course of an infection. These species can damage cellular constituents, including DNA, proteins, and lipids, leading to cellular death. The capacity to neutralize ROS represents a stress response in *Paracoccidioides,* as previously described (Chagas et al., 2008). Proteomic studies reported the up-regulation of ROS scavenging enzymes, such as peroxisomal catalase and Cu/Zn and Mn superoxide dismutases, during the treatment of *Paracoccidioides* with hydrogen peroxide, indicating the involvement of those enzymes in protecting the fungus from the general stress generated by the host defense mechanisms (Grossklaus et al., 2013). ROS detoxification has an apparent significance for virulence, as phagocytes of the innate immune system produce several oxidants that are presumed to play roles in microbial killing. In this sense, to restrict *Paracoccidioides* infection, macrophages produce several harmful substances, such as hydrogen peroxide, that cause oxidative stress (Pina et al., 2008; Rodrigues et al., 2007). The lower resistance to ROS in *Pb*EPM83, as demonstrated in the proteomic and biochemical assays, warrants further investigation.

A plethora of data have been generated from specific analyses when exposing *Paracoccidioides* to particular stressors (Silva et al., 1994, 1999; Izacc et al., 2001; Nicola et al., 2008). One

obvious stress condition every human pathogen has to endure is the elevated body temperature of the host. The isolate *Pb*EPM83 showed an over-expression of proteins characterized as HSPs. In fungi, HSPs are modulated in response to various stimuli, including temperature (Burnie et al., 2006). The abundance of HSPs in this isolate can provide this fungus the ability to survive certain environmental stresses, as demonstrated in this work.

In conclusion, we provide evidence for differential metabolic features in members of the phylogenetic complex. The data indicate a significant difference in the global metabolism in members of *Paracoccidioides*. The additional characterization of those differences may lead to the use of biochemical criteria as markers to distinguish between the four cryptic species of the genus *Paracoccidioides*. Additionally, the establishment of 2-DE reference maps for the four isolates will permit correlating the quantitative and qualitative variations in the proteomes with phenotypic characteristics such as pathogenicity, virulence and tolerance to environmental stresses.

Acknowledgments

This work at the Universidade Federal de Goiás was supported by grants from the Conselho Nacional de Desenvolvimento Científico e Tecnológico-CNPq (process numbers 558923/2009-7 and 553998/2010-5) and the Fundação de Amparo à Pesquisa do Estado de Goiás-Programa de Apoio a Núcleos de Excelência-FAPEG/PRONEX (process number 201110267000111). LLP is the recipient of a CAPES PhD fellowship. We thank Tereza Cristina Vieira de Rezende and Juliana Alves Parente for their helpful suggestions.

Appendix A. Supplementary material

Supplementary data associated with this article can be found, in the online version, at http://dx.doi.org/10.1016/j.fgb.2013.07.008.

References

Barker, B.M., Kroll, K., Vödisch, M., Mazurie, A., Kniemeyer, O., Cramer, R.A., 2012. Transcriptomic and proteomic analyses of the *Aspergillus fumigatus* hypoxia response using an oxygen-controlled fermenter. BMC Genomics 13, 62. http://dx.doi.org/10.1186/1471-2164-13-62.

Borges, C.L., Parente, J.A., Barbosa, M.S., Santana, J.M., Báo, S.N., de Sousa, M.V., Soares, C.M.A., 2010. Detection of a homotetrameric structure and protein-protein interactions of formamidase lead to new functional insights. FEMS Yeast Res. 10, 104–113.

Brummer, E., Castaneda, E., Restrepo, A., 1993. Paracoccidioidomycosis: an update. Clin. Microbiol. Rev. 6, 89–117.

Burnie, J.P., Carter, T.L., Hodgetts, S.J., Matthews, R.C., 2006. Fungal heat-shock proteins in human disease. FEMS Microbiol. Rev. 30, 53–88.

Chagas, R.F., Bailão, A.M., Pereira, M., Winters, M.S., Smullian, A.G., Deepe Jr., G.S., Soares, C.M.A., 2008. The catalases of *Paracoccidioides brasiliensis* are differentially regulated: protein activity and transcript analysis. Fungal Genet. Biol. 45, 1470–1478.

Desjardins, C.A., Champion, M.D., Holder, J.W., Muszewska, A., Goldberg, J., Bailão, A.M., Brigido, M.M., Ferreira, M.E.S., Garcia, A.M., Grynberg, M., Gujja, S., Heiman, D.I., Henn, M.R., Kodira, C.D., León-Narváez, H., Longo, L.V.G., Ma, L.J., Malavazi, I., Matsuo, A.L., Morais, F.V., Pereira, M., Rodríguez-Brito, S., Sakthikumar, S., Salem-Izacc, S.M., Sykes, S.M., Teixeira, M.M., Vallejo, M.C., Walter, M.E.M.T., Yandava, C., Young, S., Zeng, Q., Zucker, J., Felipe, M.S., Goldman, G.H., Haas, B.J., McEwen, J.G., Nino-Vega, G., Puccia, R., San-Blas, G., Soares, C.M.A., Birren, B.W., Cuomo, C.A., 2011. Comparative genomic analysis of human fungal pathogens causing paracoccidioidomycosis. PLoS Genet 7 (10), e1002345.

Felipe, M.S., Andrade, R.V., Arraes, F.B., Nicola, A.M., Maranhão, A.Q., Torres, F.A., Silva-Pereira, I., Poças-Fonseca, M.J., Campos, E.G., Moraes, L.M., Andrade, P.A., Tavares, A.H., Silva, S.S., Kyaw, C.M., Souza, D.P., Pereira, M., Jesuíno, R.S., Andrade, E.V., Parente, J.A., Oliveira, G.S., Barbosa, M.S., Martins, N.F., Fachin, A.L., Cardoso, R.S., Passos, G.A., Almeida, N.F., Walter, M.E., Soares, C.M.A., Carvalho, M.J., Brígido, M.M., 2005. Transcriptional profiles of the human pathogenic fungus *Paracoccidioides brasiliensis* in mycelium and yeast cells. J. Biol. Chem. 280, 24706–24714.

Franco, M., 1987. Host-parasite relationships in paracoccidioidomycosis. J. Med. Vet. Mycol. 25, 5–18.

Grossklaus, D.A., Bailão, A.M., Rezende, T.C., Borges, C.L., de Oliveira, M.A., Parente, J.A., Soares, C.M.A., 2013. Response to oxidative stress in *Paracoccidioides* yeast cells as determined by proteomic analysis. Microbes Infect.. http://dx.doi.org/10.1016/j.micinf.2012.12.002.

Herbert, B., Galvani, M., Hamdan, M., Olivieri, E., MacCarthy, J., Pedersen, S., Righetti, P.G., 2001. Reduction and alkylation of proteins in preparation of two-dimensional map analysis: why, when, and how? Electrophoresis 22, 2046–2057.

Izacc, S.M., Gomez, F.J., Jesuino, R.S., Fonseca, C.A., Felipe, M.S., Deepe, G.S., Soares, C.M.A., 2001. Molecular cloning, characterization and expression of the heat shock protein 60 gene from the human pathogenic fungus *Paracoccidioides brasiliensis*. Med. Mycol. 39, 445–455.

Kretschmer, M., Wang, J., Kronstad, J.W., 2012. Peroxisomal and mitochondrial β-oxidation pathways influence the virulence of the pathogenic fungus *Cryptococcus neoformans*. Eukaryot. Cell 11, 1042–1054.

Laemmli, U.K., 1970. Cleavage of structural proteins during the assembly of the head of bacteriophage T4. Nature 227, 680–685.

Matute, D.R., Sepulveda, V.E., Quesada, L.M., Goldman, G.H., Taylor, J.W., Restrepo, A., Mcewen, J.G., 2006. Microsatellite analysis of three phylogenetic species of *Paracoccidioides brasiliensis*. J. Clin. Microbiol. 44, 2153–2157.

Nicola, A.M., Andrade, R.V., Dantas, A.S., Andrade, P.A., Arraes, F.B., Fernandes, L., Silva-Pereira, I., Felipe, M.S., 2008. The stress responsive and morphologically regulated hsp90 gene from *Paracoccidioides brasiliensis* is essential to cell viability. BMC Microbiol. 8, 158.

Parente, A.F.A., Bailão, A.M., Borges, C.L., Parente, J.A., Magalhães, A.D., Ricart, C.A.O., Soares, C.M.A., 2011. Proteomic Analysis Reveals That Iron Availability Alters the Metabolic Status of the Pathogenic Fungus *Paracoccidioides brasiliensis*. PLoS ONE 6, e22810.

Parente, A.F.A., de Rezende, T.C., de Castro, K.P., Bailão, A.M., Parente, J.A., Borges, C.L., Silva, L.P., Soares, C.M.A., 2013. A proteomic view of the response of *Paracoccidioides* yeast cells to zinc deprivation. Fungal Biol. 117 (6), 399–410.

Pina, A., Bernardino, S., Calich, V.L., 2008. Alveolar macrophages from susceptible mice are more competent than those of resistant mice to control initial *Paracoccidioides brasiliensis* infection. J. Leukocyte Biol. 83, 1088–1099.

Restrepo, A., Jiménez, B.E., 1980. Growth of *Paracoccidioides brasiliensis* yeast phase in a chemically defined culture medium. J. Clin. Microbiol. 12, 279–281.

Restrepo, A., Tobon, A., 2005. *Paracoccdidioides brasiliensis*. In: Mandell, G.L., Bennet, J.E., Dollin, R. (Eds.), Principles and Practice of Infectious Diseases. Philadelphia, pp. 3062–3068.

Restrepo, A., Mcewen, J.G., Castañeda, E., 2001. The habitat of *Paracoccidioides brasiliensis*: how far from solving the riddle? Med. Mycol. 39, 233–241.

Rezende, T.C., Borges, C.L., Magalhães, A.D., de Sousa, M.V., Ricart, C.A., Bailão, A.M., Soares, C.M.A., 2011. A quantitative view of the morphological phases of *Paracoccidioides brasiliensis* using proteomics. J. Proteomics 75, 572–587.

Rodrigues, A.D.R., Dias-Melicio, L.A., Calvi, S.A., Peracoli, M.T., Soares, A.M., 2007. *Paracoccidioides brasiliensis* killing by IFN-gamma, TNF alpha and GM-CSF activated human neutrophils: role for oxygen metabolites. Med. Mycol. 45, 27–33.

Rui, B., Shen, T., Zhou, H., Liu, J., Chen, J., Pan, X., Liu, H., Wu, J., Zheng, H., Shi, Y., 2010. A systematic investigation of *Escherichia coli* central carbon metabolism in response to superoxide stress. BMC Syst. Biol. 4, 122.

San-Blas, G., Nino-Vega, G., Iturriaga, T., 2002. *Paracoccidioides brasiliensis* and paracoccidioidomycosis: molecular approaches to morphogenesis, diagnosis, epidemiology, taxonomy and genetics. Med. Mycol. 40, 225–242.

Shaw, M.M., Riederer, B.M., 2003. Sample preparation for two-dimensional gel electrophoresis. Proteomics 3, 1408–1417.

Silva, S.P., Petrofeza, S.S., Felipe, M.S.S., Soares, C.M.A., 1994. Phase transition and stage specific protein synthesis in the dimorphic fungus *Paracoccidioides brasiliensis*. Exp. Mycol. 18, 294–299.

Silva, S.P., Petrofeza, S.S., Borges-Walmsley, I., Pereira, I.S., Soares, C.M.A., Walmsley, A., Felipe, M.S.S., 1999. Differential expression of an Hsp70 gene during transition from the mycelial to the infective yeast form of the human pathogenic fungus *Paracoccidioides* brasiliensis. Mol. Microbiol. 31, 1039–1050.

Teixeira, M.M., Theodoro, R.C., Carvalho, M.J.A., Fernandes, L., Paes, H.C., Hahn, R.C., Mendonza, L., Bagagli, E., San-Blas, G., Felipe, M.S.S., 2009. Phylogenetics analysis reveals a high level of speciation in the *Paracoccidioides* genus. Mol. Phylogenet. Evol. 52, 273–283.

Teutschbein, J., Albrecht, D., Pötsch, M., Guthke, R., Aimanianda, V., Clavaud, C., Latgé, J.P., Brakhage, A.A., Kniemeyer, O., 2010. Proteome profiling and functional classification of intracellular proteins from conidia of the human-pathogenic mold *Aspergillus fumigatus*. J. Proteome. Res. 9, 3427–3442.

Theodoro, R.C., Bagagli, E., Oliveira, C., 2008. Phylogenetic analysis of PRP8 intein in *Paracoccidioides brasiliensis* species complex. Fungal Genet. Biol. 45, 1284–1291.

Untereiner, W.A., Scott, J.A., Naveau, F.A., Sigler, L., Bachewich, J., Angus, A., 2004. The *Ajellomycetaceae*, a new family of vertebrate-associated *Onygenales*. Mycologia 96, 812–821.

Vallejo, M.C., Matsuo, A.L., Ganiko, L., Medeiros, L.C., Miranda, K., et al., 2011. The pathogenic fungus *Paracoccidioides brasiliensis* exports extracellular vesicles containing highly immunogenic alpha-Galactosyl epitopes. Eukaryot. Cell 10, 343–351.

Weber, S.S., Parente, A.F., Borges, C.L., Parente, J.A., Bailão, A.M., Soares, C.M.A., 2012. Analysis of the secretomes of *Paracoccidioides* mycelia and yeast cells. PLoS ONE 7, e52470.